RESEARCH ARTICLE

Green Synthesis of Silver Oxide Nanoparticles with *Annona squamosa*

Meghaben Shah*, Ganesh Dama

SGMSPM's Sharadchandra Pawar College of Pharmacy, Otur, Affiliated to Savitribai Phule Pune University, Pune, Maharashtra, India

Received: 19th May, 2025; Revised: 30th Jun, 2025; Accepted: 16th Jul, 2025; Available Online: 25th Sep, 2025

ABSTRACT

The present investigation aims towards green synthesis and biological evaluation of nanoparticles containing silver (AgNPs) incorporated with *Annona squamosa* extracts. Optimization using Central Composite Design in Design Expert software identified ideal conditions: 1mM $AgNO_3$, 1% extract, 90-minute reaction time, and 700 rpm stirring. Extract amount and mixing time inversely influenced particle size, while $AgNO_3$ concentration and stirring speed had a direct impact. AgNPs sized 105–508 nm were stabilized by phenolic compounds. Antibacterial activity was attributed to silver ion release, which disrupted bacterial structures and functions, with Gram-negative bacteria being more susceptible. Nanoparticles under 10 nm showed enhanced cell penetration. Converting extracts into nanoparticles enhanced antimicrobial efficacy through synergistic interactions. In anticancer studies, *Annona squamosa* extract exhibited dose-dependent cytotoxicity, more effective on A431 than A375 cell lines. Nanoparticle formulations showed varied IC_{50} values depending on concentration. Overall, green-synthesized AgNPs demonstrated promising antimicrobial and anticancer potential.

Keywords: Green synthesis, Silver nanoparticles, *Annona squamosa,* antimicrobial activity, Cytotoxicity, Central Composite Design.

How to cite this article: Meghaben Shah, Ganesh Dama. Green Synthesis of Silver Oxide Nanoparticles with *Annona squamosa*. International Journal of Drug Delivery Technology. 2025;15(3):1279-92. doi: 10.25258/ijddt.15.3.49

Source of support: Nil.

Conflict of interest: None

INTRODUCTION

With its widespread use in environmental science, agriculture, and medicine, nanotechnology has become a disruptive force in many scientific domains. Because of their distinct physicochemical characteristics, metal oxide nanoparticles has emerge as potential system among the many different types of nanosystems. Particularly, silver oxide nanoparticles (AgO NPs) have concerned responsiveness due to their strong antibacterial and anticancer properties[1]. However, traditional synthesis techniques frequently use energy-intensive procedures and hazardous chemicals, which may be injurious to the atmosphere and human health. This has made it necessary to investigate new environmentally friendly and sustainable methods for nanoparticles. An eco-friendly alternative to harmful chemicals, green synthesis makes use of plant extracts and other biological resources to create these desired effects[2].

The tropical plant *Annona squamosa*, sometimes referred to as the custard apple, is widely dispersed and has a variability of therapeutic uses. Active constituents including flavonoids, alkaloids, phenolics, and acetogenins, which are abundant in its leaves, fruits, seeds, and bark, have significant medicinal benefits, such as antibacterial, anticancer, antioxidant, and anti-inflammatory qualities. When it comes to the creation of nanoparticles, these phytochemicals offer two benefits: they not only convert metal ions to nanoscale particles but also give the resulting nanomaterials biological functioning. In keeping with the ideas of sustainable development and green chemistry, this makes *Annona squamosa* a capable contestant for environmentally friendly synthesis of silver oxide nanoparticles[3,4].

There is a greater demand than ever for safe, efficient, and alternative antibacterial and anticancer drugs. A major threat to world health is the rise of antimicrobial infections which remain tolerant to several drugs, which compromises the effectiveness of traditional antibiotics and antifungals. In a similar vein, tumor infections are leading cause of mortality, despite the fact that existing treatments have limitations such as drug resistance, off-target effects, and high costs. Owing to their nano structrure with enhanced surface area, nanoparticles have the ability to interact with cellular components and more efficiently pass across biological membranes, which enhances therapeutic benefits. Because of their broad-spectrum antibacterial activity and capacity to cause cytotoxicity in cancer cells via processes including reactive oxygen species (ROS) production, DNA damage, and death, silver oxide nanoparticles in particular have shown promise[5,6].

The utilization of a medicinally rich plant resource and the environmentally friendly production of functionally active nanoparticles form the basis of the current study's justification. Despite the abundance of literature on environmentally friendly silver nanoparticle production, very little is known about the production of silver oxide nanoparticles using *Annona squamosa* extract. Also, these biosynthesized Ag2O NPs have not been extensively

**Author for Correspondence: meghashah88@gmail.com*

Table 1: Coded variables for Design experiment

Independent Factors	Symbol	Low	High
Solution of metal salt (mM)	A	1	5
Concentration of Extract (%)	B	0.1	0.5
Stirring Time (Min)	C	30	90
Dependent variables (R-response)			
R-1	Particle Size		
R- 2	Poly-dispersity Index		
R -3	Zeta Potential		

studied for their biological characteristics, particularly their antifungal, antibacterial, and anticancer potential. By using the phytochemical variety of *Annona squamosa*, this study aims to provide a novel and environmentally friendly approach to producing bio-functionalized silver oxide nanoparticles that possess potent therapeutic benefits.[7,8].

The investigation aims to formulate silver oxide nano-particles by green chemistry by employing an hydroalcoholic extract of *Annona squamosa* leaves. Assessing the produced nanoparticles' anticancer effectiveness against specific human carcinoma cell lines like breast (MCF-7) and cervical (HeLa) malignancies, is another important goal. In order to clarify the fundamental processes of cytotoxicity, the study will use *in-vitro* tests to examine cell survival, morphological alterations, and apoptosis-inducing capabilities. Additionally, using common microbiological techniques like agar bore diffusion method along with minimum effective concentration (MIC) determination, the anti microbial properties towards synthesized Ag_2O NPs will be evaluated against clinically relevant test strains, for example *S. aureus*, *E. coli*, *C. albicans*, *A. niger* [9].

There are important societal and scientific ramifications to this discovery. In terms of the environment, it minimizes the ecological impact of nanotechnology by promoting the creation of sustainable nanomaterials from plant-based resources. In terms of medicine, it provides a biocompatible and reasonably priced substitute for traditional medications, possibly getting beyond present therapeutic restrictions. Combining green synthesis with biomedical applications is a progressive strategy that supports international initiatives for environmentally responsible innovation and better healthcare solutions[10].

Finally, the production of Ag_2O NPs with extract from *Annona squamosa* offers a fresh, environmentally responsible approach with potential uses in medicine. By investigating the complete therapeutic potential of biosynthesized Ag_2O NPs, this work seeks to close the gap between conventional medical knowledge and contemporary nanotechnology. The goal of the project is future development of treatments based on nanoparticles that are both environmentally friendly and efficacious through thorough characterisation and biological assessment.

MATERIALS AND METHODS

Materials

$AgNO_3$ solution (≥99.5% purity) was purchased from Sigma-Aldrich, India.A 431 and A 375 Cell lines samples received from NCCS (National center for cell Sciences), Pune.

Table 2: Experimental runs suggested by CCD

Run	A: Solution of metal salt (mM)	B: Conc. Plant Extract (%)	C: Stirring Time (min)
1	3	0.3	90
2	1	0.1	90
3	3	0.3	60
4	5	0.5	30
5	5	0.1	90
6	5	0.3	60
7	3	0.5	60
8	1	0.1	60
9	3	0.1	60
10	1	0.1	30
11	5	0.1	30
12	5	0.5	90
13	3	0.3	30
14	1	0.5	30
15	1	0.5	90
16	3	0.3	60
17	1	0.3	60

Preliminary Screening of Green Synthesis of Nanoparticles

$AgNO_3$solution(Metal salts) with 1, 3, and 5 mM concentrations were treated with *Annona squamosa* hydroalcoholic extract at 0.1, 0.3, and 0.5%. Thus prepared formulation was evaluated by spectrophotometrical analysis. The upper and lower limits of metal ions and extract concentration were selected for further study.

Green Synthesis of Ag NPs Incorporating Annona squamosa Extracts

$AgNO_3$ solution (1, 3, and 5 mM) and hydroalcoholic extract of *Annona squamosa* (0.1, 0.3, and 0.5%) were formulated by applying double distilled water. A beaker containing $AgNO_3$ solution was kept on a magnetic stirrer and hydroalcoholic extract of *Annona squamosa* was added gradually into the $AgNO_3$ solution with constant stir upto 30-90 minutes. The reduction of Ag+ to Ag was spotted through a color change. The synthesized Ag NPs were processed towards centrifugation at 10,000 rpm(15 minutes, 4 °C). The resulting pellets were given wash twice using methanol so as to eliminate any free plant extract or remaining impurities. This was followed by filtration using a 0.22 µm syringe filter. The purified sample was then lyophilized, and thus obtained powder was kept at 4 °C for subsequent characterization, including antimicrobial and cytotoxicity assessments on both normal and cancer cell lines[11].

Optimization using Central Composite Design (CCD)

The synthesis of Ag NPs was optimized by systematically varying one parameter at a time—silver salt concentration, reaction time, or plant extract concentration—while keeping the other two constant during each experimental run. This approach helped identify the most favorable conditions for efficient nanoparticle synthesis. The optimization was evaluated by looking at the zeta potential, polydispersity index, visible color changes, and particle size measurements. The CCD was used to carry out the

Table 3: Equations for final reduced model

dependent variables	Equations
Particle size	+309.51+48.67× A+36.76 ×B+77.09×C-45.92 AB+27.40 AC+ 18.97 BC-21.68 A^2 -9.71 B^2 -82.54 C^2
PDI	+0.3082+0.0568× A+0.0605×B+0.1903×C-0.0151AB++0.0686AC+ +0.0686BC-0.0188A^2 -0.0583B^2 +0.0967C^2
Zeta Potential	-24.04-2.36× A-2.06×B-14.80×C+0.7500AB--1.80AC--1.97BC-1.70A^2 +1.90B^2 -8.60C^2

Main Effects- A, B, C; Quadratic Effects- A^2 ,B^2 ,C^2 ; Interaction Effect- AB,AC, BC

Table 4: Response Variables's Summary Statistics

Response variable	Predicted Model	F value	p-value (Prob>F)	R-squared	Adjusted R-squared	R-squared Predicted
Particle Size	Quadratic	5.78	0.0153	0.8813	0.7288	0.7144
PDI	Quadratic	34.56	0.0001	0.9780	0.9497	0.8714
Zeta Potential	Quadratic	34.48	0.0001	0.9779	0.9496	0.7844

optimization. Design Expert, version 13 Trial, was used for optimization purposes throughout the research. The study's independent variables were the concentration of metal salts (A), the concentration of the extract (B), and the duration of stirring (C), while the dependent variables were the sizes of the particles (R1), the polydispersity index (R2), and the zeta potential (R3). Table 1 contains a list of coded values that were used for the experimental design. The experimental runssuggested by CCD are depicted in Table 2[12].

Characterization of Nanoparticles

UV-Vis Spectrophotometry

UV-Visible spectrophotometric examination was performed to check formation and assess stability of AgNPs by help if hydroalcoholic extract of *Annona squamosa*. The lyophilized AgNP powder was re-dispersed in methanol or double distilled water and sonicated to ensure uniform dispersion[13]. The sample was then run for analysis in the range of 300–700 nm using spectrophotometrical analysis, with methanol or water as the blank. The characteristic surface plasmon resonance (SPR) peak, typically observed between 400–450 nm, indicated the successful synthesis of AgNPs[14]. A sharp and distinct peak suggested well-dispersed nanoparticles, while broader or shifted peaks indicated possible aggregation or polydispersity. This analysis also enabled monitoring of nanoparticle formation kinetics by recording spectra at different time intervals during synthesis[15].

Dynamic Light Scattering (DLS)

To conduct a DLS study of *Annona squamosa* extract-synthesized AgNPs, the lyophilized nanoparticle powder was first re-dispersed in double distilled water, sonicated to break aggregates, and passed via 0.22 µm syringe for filtration. After stabilizing the DLS instrument and selecting the measurement mode, the sample was transferred to a clean cuvette without bubbles. Measurement parameters such as temperature (usually 25°C), scattering angle (90°), and number of runs (3–5) were set. The measurement was performed to analyze light scattering caused by nanoparticle motion[16].

X-ray Diffraction Analysis (XRD)

The lyophilized silver nanoparticle powder was gently ground to obtain a fine, homogeneous sample. The powdered sample was placed onto a clean sample holder or glass slide, ensuring an even and flat surface. The sample holder was loaded into the XRD instrument. The XRD analysis was done using radiation of Cu-Kα (wavelength ~1.5406 Å) and range suitable for AgNPs (typically 2θ = 20°–80°). Diffraction patterns were recorded, and the characteristic peaks corresponding to crystalline silver were identified. The data were analyzed to determine the crystalline structure, phase identification, and average crystal size using the Debye-Scherrer equation.

Fourier Transform Infrared Spectroscopy (FTIR)

A small amount of lyophilized silver nanoparticle powder was mixed with KBr in an appropriate ratio (usually 1:100). The ingredients were crushed to a fine powder and then compressed into an opaque pellet by use of a hydraulic press. In the sample holder, the pellet was inserted.The spectral were recorded over the range of 4000 to 400 cm^{-1}. The obtained spectra then check to identify functional groups and biomolecules from the *Annona squamosa* extract involved in the reduction and stabilization of AgNPs by observing characteristic absorption peaks.

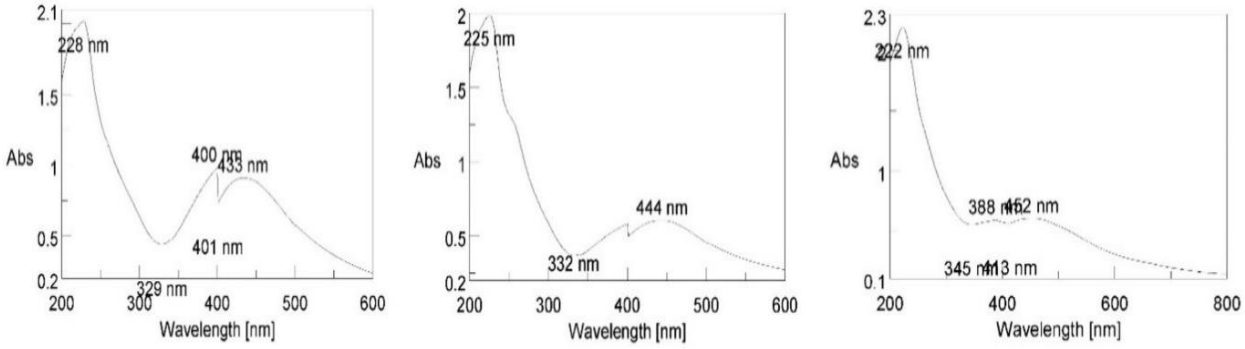

Figure 1: Preliminary Screening for Silver nitrate and Black tea extract

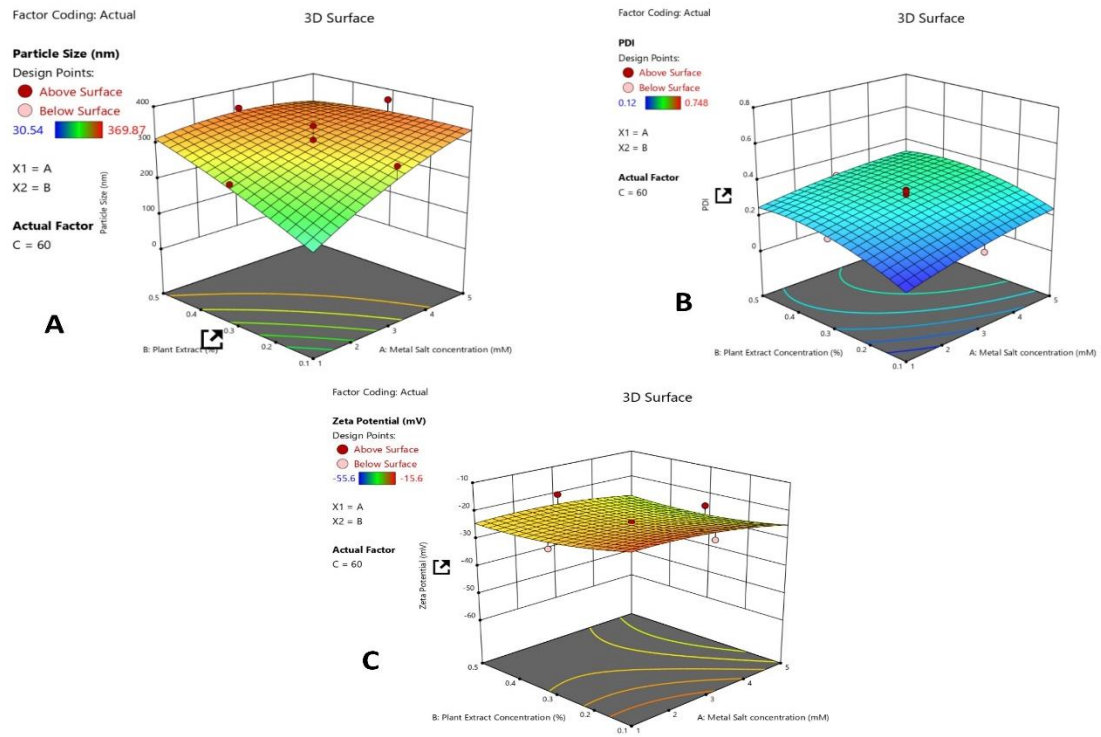

Figure 2: 3D Response surface plot (A) Effect of concentration of metal salt and concentration of extract on particle size, (B) Effect of concentration of metal salt and concentration of extract on PDI (C) Effect of concentration of metal salt and concentration of extract on Zeta Potential

Scanning Electron Microscopy (SEM)

For SEM analysis,centrifugation was carried out at 14,000 rpm upto 4 min on solution of colloids. Then resulting pellet was put in deionized water and centrifuged for 3-4 min, with this washing step repeated three times. The final pellet was rinsed with acetone to ensure purity. The cleaned AgNP's were then made into uniform suspension after 10 minutes of sonication. About an ml of the suspension was kept on a sample grid to dry completely under a lamp. During SEM imaging, a high-energy electron beam was focused on the nanoparticle surface, and the resulting backscattered electrons were used to reveal detailed surface characteristics of the sample.

Transmission Electron Microscopy (TEM)

A small quantity of lyophilized silver nanoparticle powder was re-dispersed in double distilled water or an appropriate solvent by gentle sonication. Around 1 ml of well-dispersed nanoparticle sample in suspension from was mounted to TEM grid made up of carbon-coated copper. Excess sample was scrapped using filter paper and dried at room temperature. The dried sample grid was loaded into the TEM instrument. TEM images were captured at suitable accelerating voltages to observe the surface characteristics, size, and distribution of AgNPs. The images then analyzed to measure particle size and shape, confirming nanoparticle formation.

In-vitro Antifungal Activity of Extract and Ag-NPs

This was assessed by employing the diffusion method with agar bore well using *Aspergillus niger* and *Candida albicans as a test species*. Both fungal strains were cultured onto PDA plates to incubate (30 °C, 3–5 days). A suspension was then made in sterilized phosphate-buffered saline (PBS, pH 7) with spore concentration upto 10^7 spores per mL using a cell counting chamber. One milliliter of this suspension was evenly spread over MEA agar plates. Wells of size 8 millimeter in diameter were bored with a presterilizes sterile cork borer. Around 100.00 µL of hydroalcoholic plant extracts or AgNPs synthesized from both plants were added separately to it, and kept (4 °C, 2 hr) before incubation. Itraconazole and Fluconazole served as the reference antifungal agent, and incubation temperature maintained at 30 °C upto 3 days. Following incubation, the zones of inhibition were measured and documented. Additionally, various concentrations of the hydroalcoholic extract and AgNPs were tested for their antifungal activity to determine MIC.The results (in triplicate) were presented as mean SEM.

Minimum Inhibitory Concentration (MIC)

The method for diluting broth that is recommended by the CLSI (M07-A8). This included keeping an eye on the observable development of bacteria in broth culture. The AgNPs and extracts were diluted in BHI broth in steps ranging from 31.25 µg per mL to 1000 µg per mL. The bacterial suspensions were adjusted to 10□ Colony Forming Units per mL. One set of experiments was incubated at 37 °C for 24 hours with only the inoculation broth as a control. When no discernible microbial growth was seen at a certain dose, this was called MIC. The MIC values were confirmed by visually observing the tubes before and after incubation for turbidity.

In-vitro Anti-bacterial Activity of Extract, AgNPs

This can be evaluated using the agar bore well diffusion technique. Bacteria culture were first subcultured in broth to incubate (37 °C , 24 hr). The overnight cultures was evenly spread onto agar plates to ensure uniform microbial lawn formation. The tested bacterial strains included *E. coli*

(Gram--ve) and *S. aureus* (Gram+ve). For analysis, silver nitrate, plant extracts, and standard antibiotics streptomycin and Gentamycin were used as control treatments.

Wells were created in the agar using a pre-sterilized cork and borer, and specific concentrations of the test samples and standards were introduced into each well and incubated (37 °C/24 hr). Inhibition zones around each well was measured and compared with those of the control treatments. The results of the triplicate study were presented as mean SEM[17].

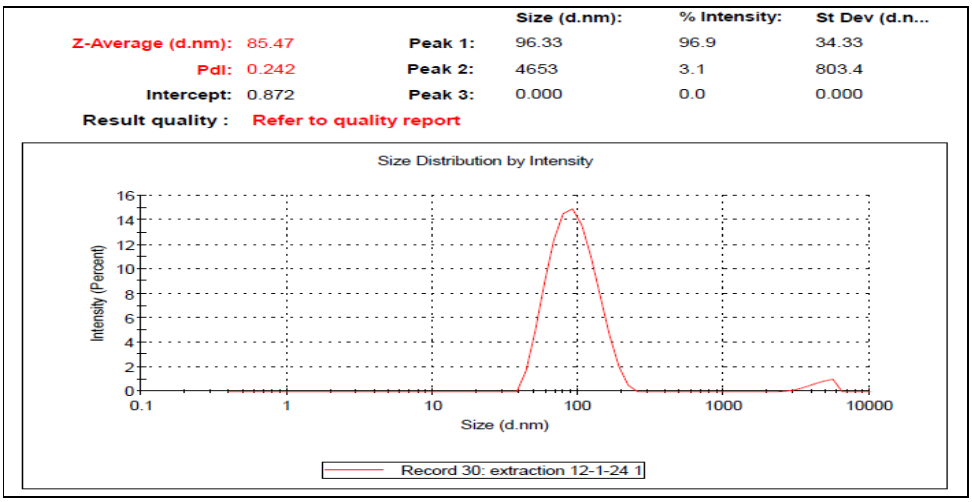

Figure 3: Dynamic light scattering (DLS) measurements were done to determine the size of the AgNP

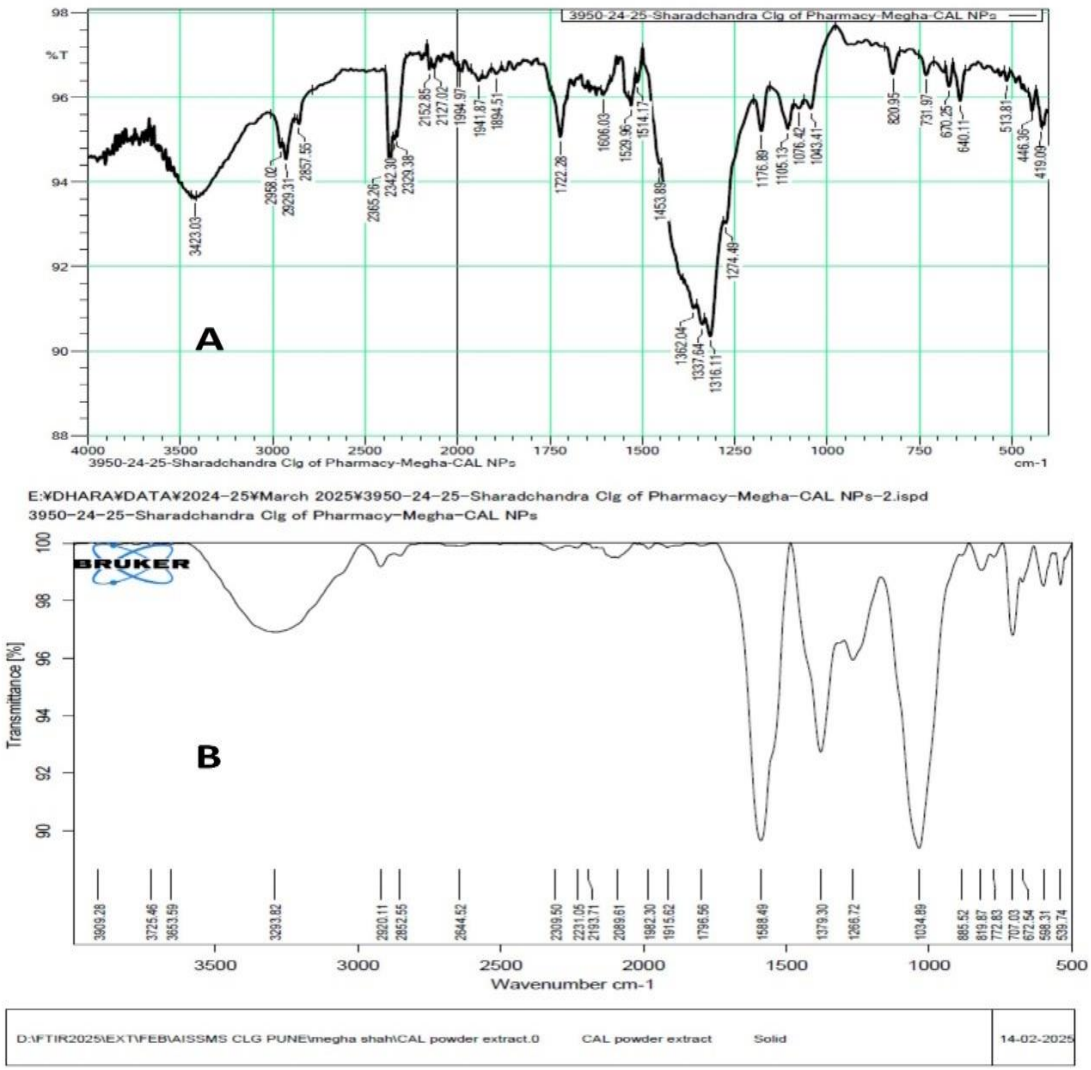

Figure 4: FTIR spectra (A) ASL hydroalcoholic Extract, (B) AgNPs of ASL Hydroalcoholic extract

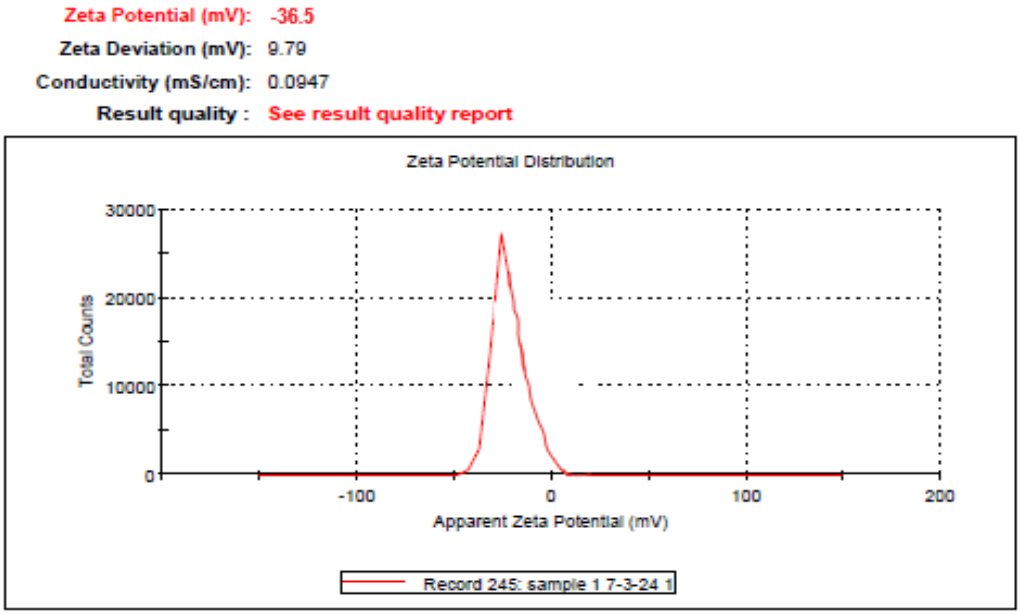

Figure 5: Zeta Potential analysis of Ag NP's

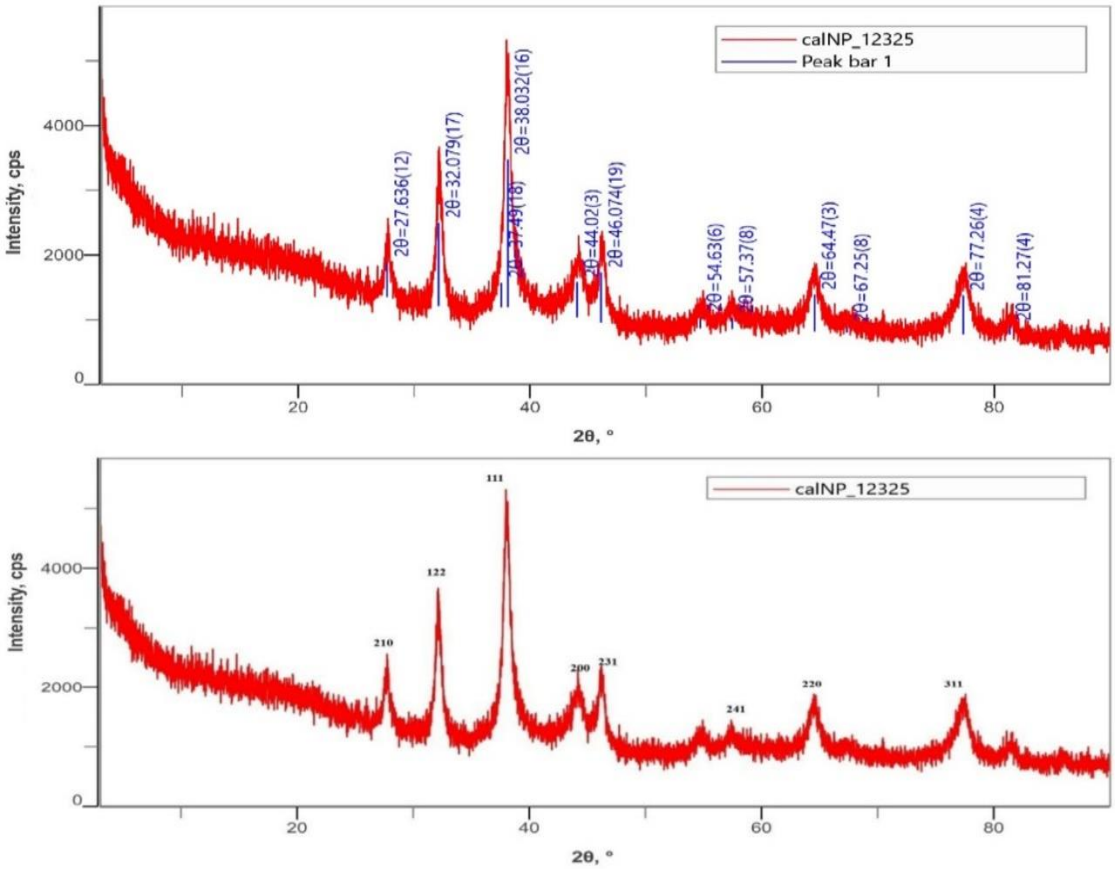

Figure 6: XRD analysis of Ag NP's

Cell Line Study using A 431 and A 375 cells

Maintenance of Cell Lines

Complete growth medium was used for the routine subculturing of A431 and A375 cell lines. This media included 89 mL of DMEM (Himedia, Ref: AL250A), 10.00 mL of FBS (Himedia, RM10432, Lot 573421), and 1 mL of antibiotics (Himedia, A002, Lot 5392281) up to 100 mL[18]. Using an inverted light microscope, the cells were observed on a regular basis while incubated in a CO_2 atmosphere maintained at 5%. The next step was to culture the samples in a Class II cabinet that was specifically designed to exclude any possibility of microorganisms. At 85% confluency, trypsin (TCL007, LOT 536691) was administered as a therapy[19]. Subculturing was carried out in accordance with the established procedure. As a reference for skin cancer cell lines, theHaCaT human

keratinocyte line is a typical cell line.

Preparation of Dulbecco's Modified Eagle Medium (DMEM) Medium

In a beaker, dissolve 13.3 g of DMEM powder in 900 mL of double-distilled water. Keep the temperature between 15 and 30 °C as you prepare the mixture. After that, 3.0 g of sodium bicarbonate was added, and to modify the pH of the solution, 1 mN NaOH or 1 mN HCl were used as required. The final pH was carefully controlled to be between 7.60 and 8.20. Cell culture applications subsequently made use of the sterile media[20].

MTT Assay

This was conducted at log growth phase. A 96-well plate was marked accordingly, including wells designated as negative controls (without the addition of any test compound). Viable cell counts were fixed using the exclusion method using trypan blue. Cells then seeded (density equal to 5×10^3 cells per well) complete growth

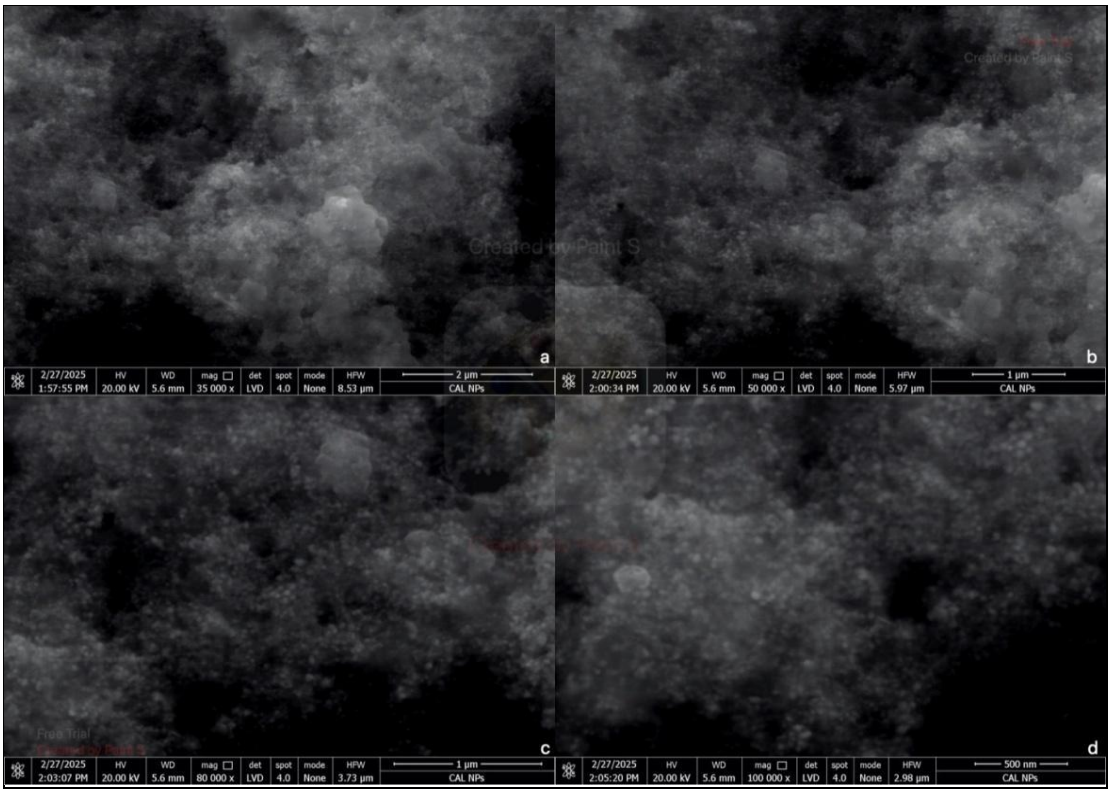

Figure 7: SEM image of Ag NP's

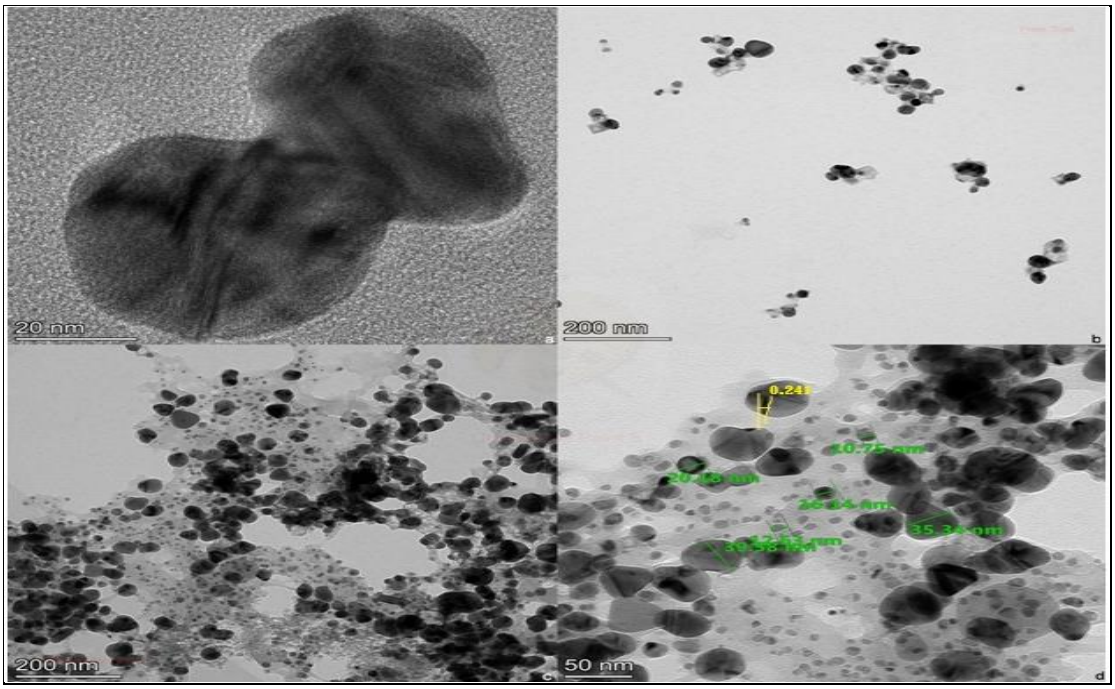

Figure 8: TEM image of Ag NP's

Table 5: Antifungal activity of ASL HAE extracts, ASL HAE AgNPs on *Aspergillus niger* and *Candida albicana*

Sample	Fungal Strain	Zone of inhibition (mm ± SEM)	
		Hydroalcoholic extract	Hydroalcoholic extract AgNps
Annona squamosa Leaves	*Aspergillus niger*	12.3±0.5	15 ± 0.6
	Candida albicana	12.0±0.7	14.5±0.5
Standard Itraconazole	*Aspergillus niger*	19.75 ±0.25	
	Candida albicana	16.75 ±1.25	
Standard Fluconazole	*Aspergillus niger*	18.30 ±0.70	
	Candida albicana	19.50 ±1.50	
DMSO Negative control	*Aspergillus niger*	9±0.01	
	Candida albicana	9±0.01	

SEM = Standard error mean, P=0.023*

Table 6: Antibacterial activity of ASL HAE and , ASL HAE AgNPs-on *Staphylococcus aureus* and *Escherichia coli*

Sample	Fungal Strain	Zone of inhibition (mm ± SEM)	
		Hydroalcoholic extract	Hydroalcoholic extract AgNps
Annona squamosa Leaves	*Staphylococcus aureus*	10.6±0.5	12.5 ± 0.6
100 µg/ml	*Escherichia coli*	10.0±0.7	12.3 ±0.5
Standard Streptomycin	*Staphylococcus aureus*	29.60 ±0.40	
1000µg/ml	*Escherichia coli*	31.60 ±1.40	
Standard Gentamycin	*Staphylococcus aureus*	33.50 ±0.50	
1000 µg/ml	*Escherichia coli*	36.00 ±1.00	
DMSO Negative control	*Staphylococcus aureus*	9±0.01	
	Escherichia coli	9±0.01	

SEM = Standard error mean, P=0.020*

medium was added to bring the total volume to 150 µL per well. After incubating for 24 hours in a 5% CO_2 incubator to allow cell attachment and entry into the log phase, varying concentrations of the test compound (1000 to 31.25 µg per mL) added in a serial dilution format. The plate was then kept to incubate upto 24 hr.

After incubation, remnant media from each well was then carefully removed to replace with fresh medium. After this time lapse around 20 µL of MTT reagent mixed with media and then added to each well. To protect the photosensitive MTT dye, the aluminium foil was used for wrapping to incubate for 4 hrs. The resulting supernatant was gently decanted without disturbing the formazan crystals that About 100 µL of DMSO and µL of glycine buffer were mixed to add in order to solubilize the crystals . Absorbance was checked on spectrophotometer (570 nm). The proliferative index was calculated by dividing the optical density (OD) of the test samples by the OD of the control, then multiplying by 100[21].

$$\text{Percentage (\%) of Cell viability} = \frac{\text{A570 of treated cells}}{\text{A570 of control cells}} \times 100$$

Each concentration of hydroalcoholic extracts of the plant, its NPs were independently assayed three times with three technical replicates for both the A431 and A375 cell lines.

RESULTS AND DISCUSSION

Preliminary Screening for Synthesis of Nanoparticles

Fron results observed it can be stated that a conc. of extract and silver nitrate played a vital part in the synthesis of AgNPs (Figure 1). Synthesis of AgNPs with 0.1, 0.3, and 0.5 % concentrations of ASL hydroalcoholic extract and 1, 3, and 5 mM of $AgNO_3$ was successfully done. UV spectroscopy results revealed that the UV peak intensity increased with the increases with concentrations of metal salt and ASL extract. Any of the characteristic peaks of AgNPs were not observed below 0.5 mM concentration of silver nitrate. From the results, it was concluded that a concentration below 0.5 mM was insufficient to form the AgNPs, and there is a direct relationship between metal salt concentration and plant extract concentration.

Concentrations above 5 mM resulted in a redshift of the UV peak from 433 nm to 452 nm. Smaller AgNPs displayed a UV-Vis absorption band in the range of 400–450 nm, while an increase in particle size caused the band to shift toward higher wavelengths, typically between 450 and 495 nm. The size of nanoparticles significantly affects photon excitation and band formation. Additionally, variations in the size of AgNPs have a notable impact on their color change. The development of large-sized nanoparticles was suggested by the redshift in the UV peak. The explanation for this is that the availability of silver ions increases with increasing silver nitrate concentration, which raises the rate of the reaction. It leads to a rise in AgNPs production. As a result of the increased synthesis, AgNPs aggregate and grow into larger particles. For this reason, 0.1 to 0.5% ASL extract and 1 to 5mM $AgNO_3$ concentration were used for the optimization investigation[24].

Optimization using CCD

Explanation of Regression Analysis

The variation in particle size, PDI, zeta potential of AgNPs was evaluated using response surface methodology, as these properties depend on nanoparticle composition. Statistical analysis, including ANOVA, was conducted to identify the best-fit quadratic models, with greater values of F and lower p-values ($p < 0.05$) indicating significant

effects of the formulation variables. The study examined the influence of metal salt (A) and plant extract (B) concentrations while keeping the reaction time constant at 90 minutes. Results showed that increasing both A and B led to higher particle size, PDI, and zeta potential. Optimal nanoparticle characteristics—smaller size, lower PDI, and stable zeta potential—were achieved with lower concentrations of both metal salt and plant extract.The derived equations for particle size, PDI and zeta potential shown in Table 3.

Regression coefficients (R^2), regression value (p-value) and are shown in Table 4.

Effect of Independent Variables on Dependable Variables Interms of 3D Response Surface Plots Interpretation

The effect of independent factors on particle size, PDI, and zeta potential was illustrated through graphical analysis. During AgNP synthesis, plant extract reduces silver nitrate to form metallic silver atoms, which act as nuclei for nanoparticle formation. These nuclei are stabilized by phytoconstituents from the extract, which serve as capping agents to prevent agglomeration. As reaction time progresses, the nuclei grow, and according to the rule of mass action, higher plant extract concentrations increase reaction rates and yield. This rapid reaction facilitates immediate capping of silver atoms, leading to smaller particle sizes. Similarly, lower silver nitrate concentrations result in smaller particles due to sufficient capping by phytochemicals. However, at higher silver nitrate concentrations with limited capping agents, agglomeration occurs, producing larger nanoparticles.

Independent factors impact on particle size, PDI and Zeta Potential is shown in the Figure 2.

As shown in Figure 2, the impact of metal salt concentration (A) and plant extract conc. (B) on particle size, polydispersity index (PDI), and zeta potential of AgNPs with processing time (C) held constant at 60 minutes. Results show that increasing both A and B leads to a significant rise in particle size and PDI, indicating larger and more heterogeneous nanoparticles. The smallest particle size (~30.54 nm) and lowest PDI (~0.12) were

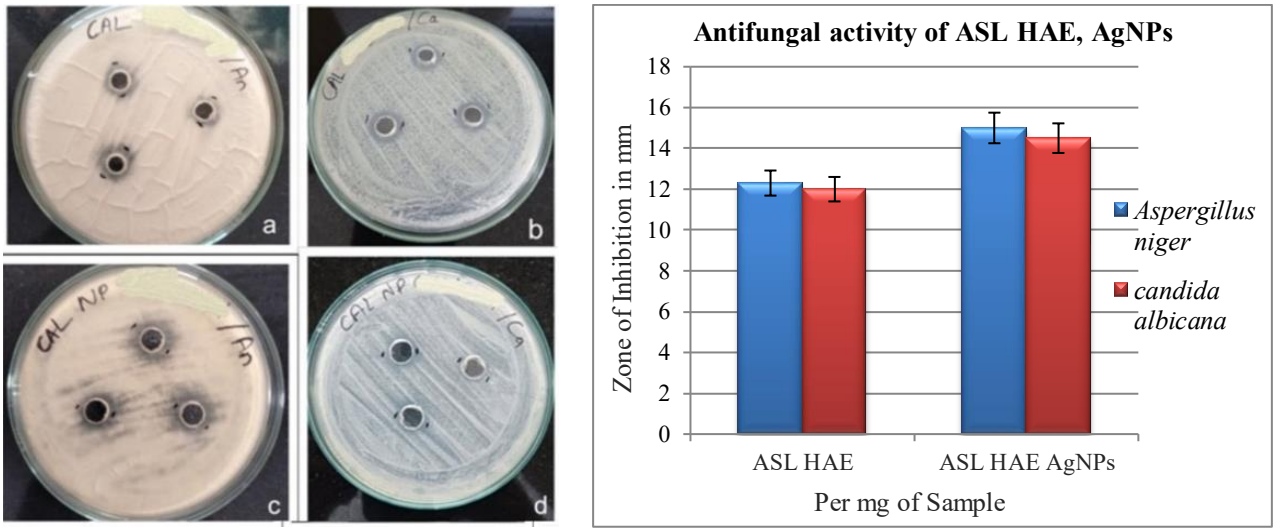

Figure 9: Zone of Inhibition (A) ASL HAE against An, (B) ASL HAE against Ca,(C) ASL HAE AgNPs against An, (D) ASL HAE AgNps against Ca, along with graphical representation for antifungal activity

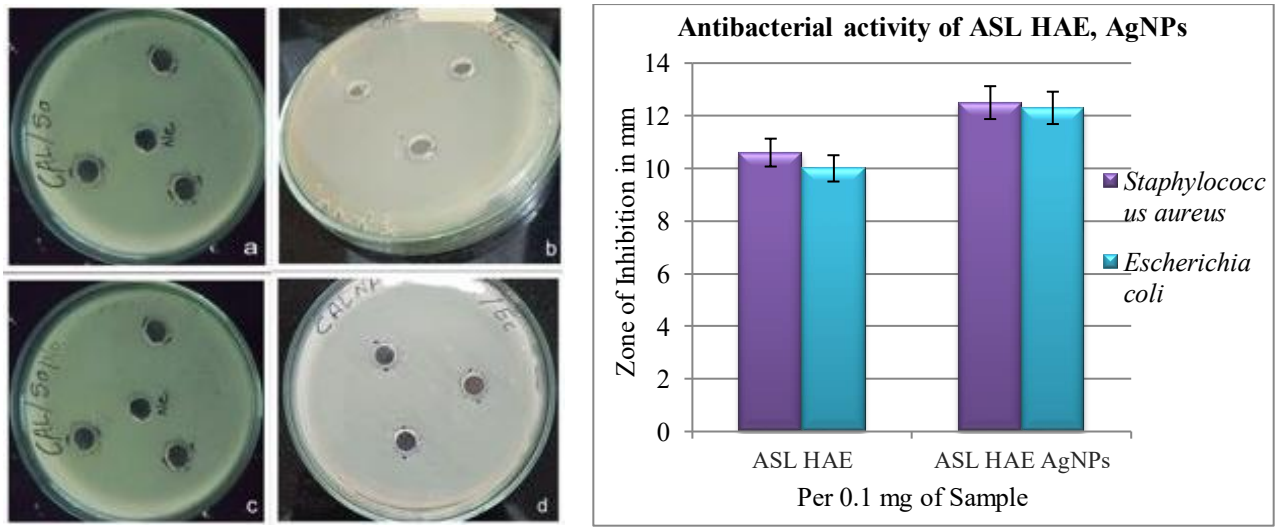

Figure 10 : Zone of Inhibition (A) ASL HAE against Sa, (B) ASL HAE against Ec, (C) ASL HAE AgNPs against Sa, (D) ASL HAE AgNPs against Ec) and concentration of sample along with graphical representation for antibacterial activity

observed at low concentrations of both components, while higher concentrations resulted in particle sizes up to ~3698.7 nm and a PDI of ~0.748, likely due to aggregation from insufficient capping.

Zeta potential values found to be −36.3 mV. Here more negative values observed at lower concentrations, suggesting better stability. As A and B increased, zeta potential became less negative, indicating reduced nanoparticle stability and a higher likelihood of aggregation. Overall, the study highlights that lower concentrations of metal salt and plant extract favor the formation of smaller, more uniform, and stable AgNPs, emphasizing the importance of optimizing formulation parameters.

UV-Vis Spectrophotometry

A preliminary confirmation of silver nanoparticle (AgNP) synthesis was observed through a color change to brown, indicating the reduction of Ag^+ to Ag^0 by plant extract phytochemicals, particularly polyphenols, which act as both reducing and stabilizing agents. UV-Vis spectroscopy was used to monitor nanoparticle formation, with a characteristic Surface Plasmon Resonance (SPR) peak observed at 444 nm, confirming AgNP synthesis. The polyphenols themselves showed a UV absorption peak at 278 nm[22,23].

UV-Vis spectra at various time intervals (30, 60, 90 minutes). An increase in SPR peak intensity over time indicated ongoing reduction of silver ions and continuous nanoparticle formation. However, as reaction time extended, a decrease in peak intensity was observed, suggesting depletion of phytochemicals. Additionally, peak broadening and a red shift (toward higher wavelengths) were noted, indicating an increase in particle size due to agglomeration over time[24].

DLS

This was conducted to evaluate the size of the synthesized AgNPs. The particle size distribution curve, illustrated in Figure 3, revealed that the nanoparticles from 50 nm to 130 nm (85.47 nm as average). The size variation between the smallest and largest particles was 80 nm. The measured polydispersity index (PDI) was 0.242, indicating a monodisperse system with a narrow size distribution. A PDI value below 0.5 generally signifies that the nanoparticles have a uniform size distribution[25].

FTIR

The study was conducted to identify the functional groups involved in the synthesis and stabilization of AgNPs.

The spectra of the ASL hydroalcoholic extract exhibited key peaks at 3293 and 2920 cm^{-1} (O–H stretching), 1588 cm^{-1} (N–H bending or NO_2 stretching), 1379 cm^{-1} (O–H bending or C–F stretching), 1034 cm^{-1} (S=O stretching), and 672 cm^{-1} (C=C bending). The AgNPs spectrum showed similar peaks at 3423 and 2952–2929 cm^{-1} (O–H stretching), along with new peaks at 1722 cm^{-1} (C–H bending, aromatic), 1316 cm^{-1} (S=O or C–F stretching), 1179 cm^{-1} (C–N stretching), and 640 cm^{-1} (C=C bending). The $AgNO_3$ spectrum displayed a broad band at 1362 cm^{-1} due to NO_3^- stretching (Figure 4).

Zeta Potential Measurement

Table 7: Effect of *Annona squamosa* leaves hydroalcoholic extract (ASL HAE), hydroalcoholic extract AgNps (ASL HAE AgNPs), on A 431 Cell line and A 375 cell line

S. No.	Concentration (µg/ml)	% Cell Viability			
		A 431 cell line (Non melanoma cell line)		A375 cell line (Melanoma cell line)	
		ASL HAE	ASL HAE AgNPs	ASL HAE	ASL HAE AgNPs
1	31.25	88.6	78.3	86.6	88.6
2	62.5	83.6	69.5	80.8	83.6
3	125	80.4	66.8	78.6	80.4
4	250	66.2	57.2	74.7	66.2
5	500	55.4	42.1	64.5	55.4
6	1000	48.3	40.1	59.4	48.3
	IC_{50} value	757.3	570.2	1634	841.3

Standard drug Cisplatin IC50: 52 (µg/ml)

Furthermore, the zeta potential, was measured to be −36.5 mV, indicating good stability. Zeta potential crucial in determining both the stability and skin permeation potential of AgNPs. Values exceeding ±30 mV typically reflect strong electrostatic repulsion, which helps prevent the aggregation of similarly charged nanoparticles within a suspension. The observed negative zeta potential suggests effective repulsion among the AgNPs, contributing to their stability and minimizing the risk of agglomeration. This finding aligns with previous results obtained for AgNPs synthesized using ASL leaf extract. The negative charge is likely attributed to the capping effect of bio-active entity present in the ASL extract. So,present results show a good dispersion state of NPs in liquids (Figure 5).

XRD

This study confirmed the crystalline nature and nanoscale size of the synthesized AgNPs. The observed diffraction peaks correspond to various crystallographic planes, with dominant reflections at 2θ = 38.03°, 44.02°, 64.47°, and 77.26°, associated with the (111), (200), (220), and (311) planes, respectively—typical of silver's face-centered cubic (FCC) structure (Figure 6).

Additional peaks such as (210), (122), (231), and (241) suggest the presence of less common facets or minor impurities. The calculated interplanarspacings and peak positions align with standard silver patterns, confirming phase purity. Crystallite sizes, determined using the Scherrer equation, ranged from 61 Å to 139 Å (6.1–13.9 nm), indicating successful formation of nanocrystals. Peak broadening, particularly in higher angle peaks, reflects the small size and lattice strain characteristic of nanoparticles. Overall, the XRD results validate the synthesis of well-defined, nanocrystalline silver particles with a predominantly FCC structure.

SEM

At the Sicart Research Lab at Vallabh Vidyanagar, SEM analysis was performed on the produced AgNPs using a Field Emission Gun Scanning Electron Microscope (FEG-SEM 450) with EDAX. Using four different magnifications, SEM images of AgNPs manufactured using ASL hydroalcoholic extract are shown in Figure 7. As seen in Figure 7a, small nanoparticles under 100 nm are present.

However, Figure 7b reveals significant agglomeration, with particles forming larger aggregates ranging from 500 nm to 2 µm. These loosely bound nanoclusters may consist of individual nanoparticles that either failed to fully coalesce or are fragments of larger particles. This observation supports the conclusion that ASL extract plays a key role as both a reducing and capping agent in the formation and stabilization of AgNPs.

TEM

This study was conducted at 200 kV (Tecnai 20, Philips, Holland) at Sicart Research Lab, VallabhVidyanagar, Gujarat, to further analyze the morphology, size, and crystallinity of AgNPs synthesized using ASL hydroalcoholic extract. The high-resolution TEM images showed the AgNPs are mostly sphere shaped (average diameter 20 - 50 nm). Some agglomerates and individual dispersed nanoparticles were also observed, supporting findings from SEM and FESEM analyses. Additionally, HRTEM images showed clear lattice fringes with an interplanar spacing of 0.241 nm, corresponding to the (111) plane of metallic silver, further validating their crystalline nature (Figure 8).

Stability of ASL-Ag NP

This was evaluaetd under ambient, dark storage conditions over six months. Post-synthesis, centrifugation was performed to remove unreacted biological materials and minimize agglomeration. UV–Vis spectroscopy (200–800 nm) was used to monitor stability at regular intervals. Results showed no significant change in absorbance spectra during the first 30 days. After this period, a decrease in intensity and sharper peak suggested initial agglomeration, while by six months, slight peak broadening indicated minor aggregation. Despite these changes, the peak position remained unchanged throughout, confirming the high stability of the biosynthesized AS-AgNPs.

In-vitro Antifungal Study

It was assessed various formulations derived from ASL hydroalcoholic extract (ASL HAE) was evaluated against *Aspergillusniger* and *Candida albicans*, with results expressed as zones of inhibition in millimeters. AgNPs synthesized from the same extract demonstrated enhanced antifungal efficacy, with zone of inhibition of 15 ± 0.6 mm for *A. niger* and 14.5 ± 0.5 mm for *C. albicans*, indicating improved potency due to nanoparticle formulation. Among the standards, itraconazole and fluconazole exhibited the greatest antifungal action(ZOI as 16.75 to 19.75 mm) serving as positive controls. The negative control (DMSO) showed minimal activity (9 ± 0.01 mm), confirming the observed antifungal effects were due to the active compounds. Overall, the results highlight the significant antifungal potential of AgNPs synthesized from ASL extract (Table 5 and Figure 9).

The antifungal activity observed across various formulations stems from their unique physicochemical characteristics and modes of action. AgNPs showed enhanced efficacy owing to their nanoscale size, increased surface area, and ability to generate reactive oxygen species and release Ag^{+} ions, leading to fungal cell damage. Standard antifungal drugs (itraconazole and fluconazole) demonstrated the highest inhibition, validating their targeted action on fungal cell membranes. The negligible activity of DMSO confirmed that the antifungal effects were attributable to the active components. Overall, the results emphasize the potent antifungal potential of AgNPs

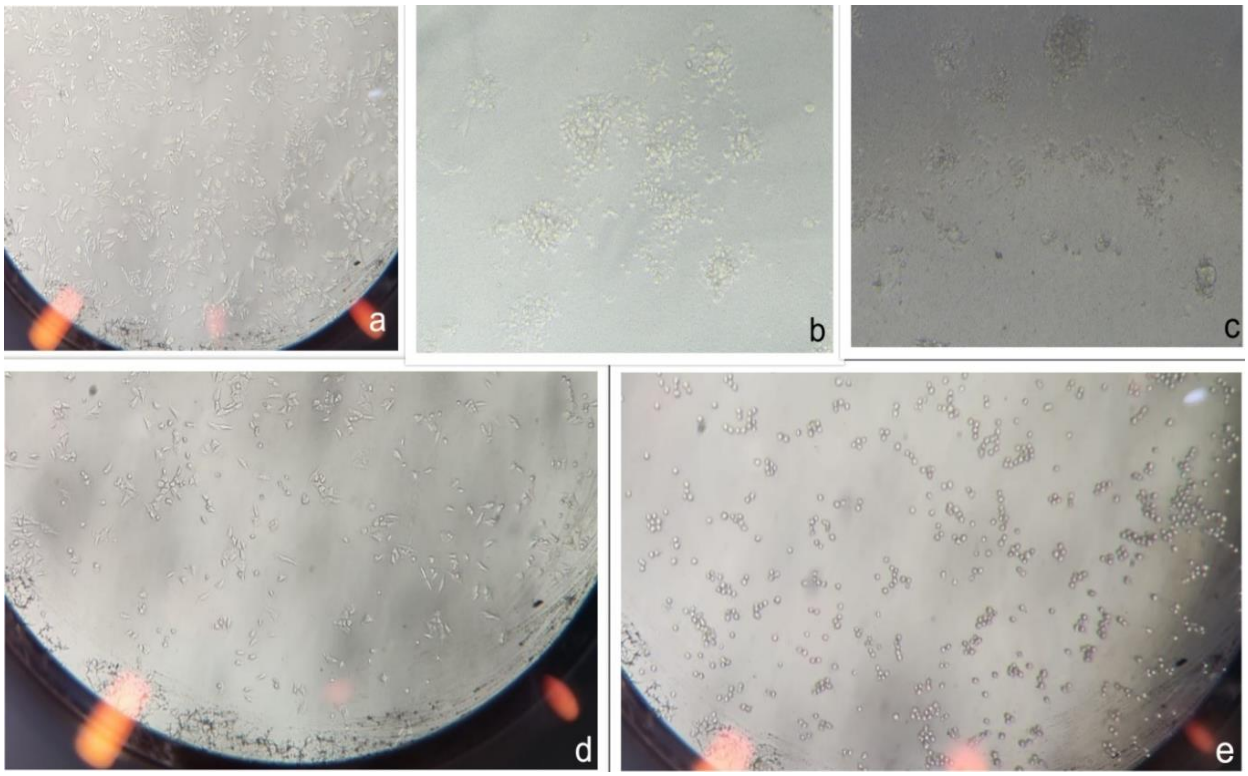

Figure 11: Effect on Cell line, (A) Normal Control, (B) *Annona squamosa* HAE effect on cell line A 431 , (C) *Annona squamosa* HAE AgNPs effect on cell line A 431, (D) *Annona squamosa* HAE effect on cell line A 375 , (E) *Annona squamosa* HAE AgNPs effect on cell line A 375

and the crucial role of formulation in modulating bioactivity.

In-vitro Antibacterial Activity

The antibacterial effects of the ASL HAE and its synthesized AgNPs were tested on *S. aureus* and *E. coli*, with the results expressed as ZOI diameters at a conc. of 100 µg per mL (Table 6 and Figure 10). An ASL extract showed moderate anti-bacterial potential, producing ZOI of 10.6 ± 0.6 mm for *S. aureus* and 10.3 ± 0.7 mm for *E. coli*. The minimum inhibitory concentration (MIC) for both bacterial strains was determined to be 250 µg/ml.

ASL-based formulations exhibited noteworthy antibacterial activity, underscoring their potential as effective natural therapeutics. While the inhibition zones were comparatively smaller than those of standard antibiotics like streptomycin and gentamycin (29.6 to 36.0 mm), the ASL formulations still produced substantial zones of inhibition, clearly surpassing the negative control (DMSO, 9 ± 0.01 mm). It has been observed that Hydroalcoholic extract and Hydroalcoholic extract AgNps showed better zone of inhibition at lower concentration (100 µg per ml) as compared to standard (1000 µg per ml). This confirms that the anti-bacterial effect was a direct result of the bioactive compounds present in the ASL extract. These encouraging results highlight the promise of ASL-based systems as safer, plant-derived alternatives to conventional antibiotics, with further scope for enhancement through formulation optimization and combination strategies.

AgNPs exhibit anti-bacterial action throughia numerous ways, primarily by releasing Ag^+on bacterial cell walls and membranes, enhancing their permeability and disrupting structural integrity. ROS also contribute to membrane damage and genetic disruption. Gram-ve bacteria are largely susceptible due to their thinner cell walls, which allow easier nanoparticle penetration compared to gram-positive bacteria. AgNPs smaller than 10 nm are particularly effective due to their enhanced ability to enter cells. Furthermore, plant extracts like *Annona squamosa* show intrinsic antimicrobial activity, which is significantly enhanced when converted into AgNPs. This increased efficacy is attributed to synergistic interactions between Ag^+ ions and phytochemicals, along with the high surface area of the biosynthesized nanoparticles that facilitates better interaction with bacterial cells.

In-vitro Skin Cancer Cell Line

Anticancer Effect of Annona squamosa Hydroalcpholic Extract on Skin Cancer Cell Lines A 431

According to Table 7, the cell viability was 78.3%, 69.5%, 66.8%, 57.2%, 42.1%, and 40.1% at concentrations of 31, 25, 6, 12, 25, 250, 500, and 1000 µg/ml of *Annona squamosa* hydroalcoholic extract, which had an anticancer impact on skin cancer cell lines A431. Thus, at a concentration of 757.3 µg/ml, the hydroalcoholic extract of *Annona squamosa* exhibited half of the maximum inhibitory concentration. cytotoxicity assessment of *Annona squamosa* hydroalcoholic extract revealed a dose-dependent decline in cell viability, with higher concentrations (250–1000 µg/ml) showing increased toxicity and lower viability percentages. At lower concentrations (31.25–125 µg/ml), the extract exhibited mild cytotoxic effects, indicating relative safety at therapeutic doses.

The IC_{50} value of 757.3 µg/ml suggests moderate cytotoxicity, requiring a relatively high concentration to inhibit 50% of cell viability. A slight variation in cell viability at 1000 µg/ml between replicates points to possible experimental variability. Overall, the extract demonstrates moderate cytotoxic potential, supporting its cautious use in biomedical applications.

Anticancer Effect of Annona squamosa Hydroalcoholic Extract NPs on Skin Cancer Cell Lines A431

Skin cancer cell lines treated with *Annona squamosa* HAE

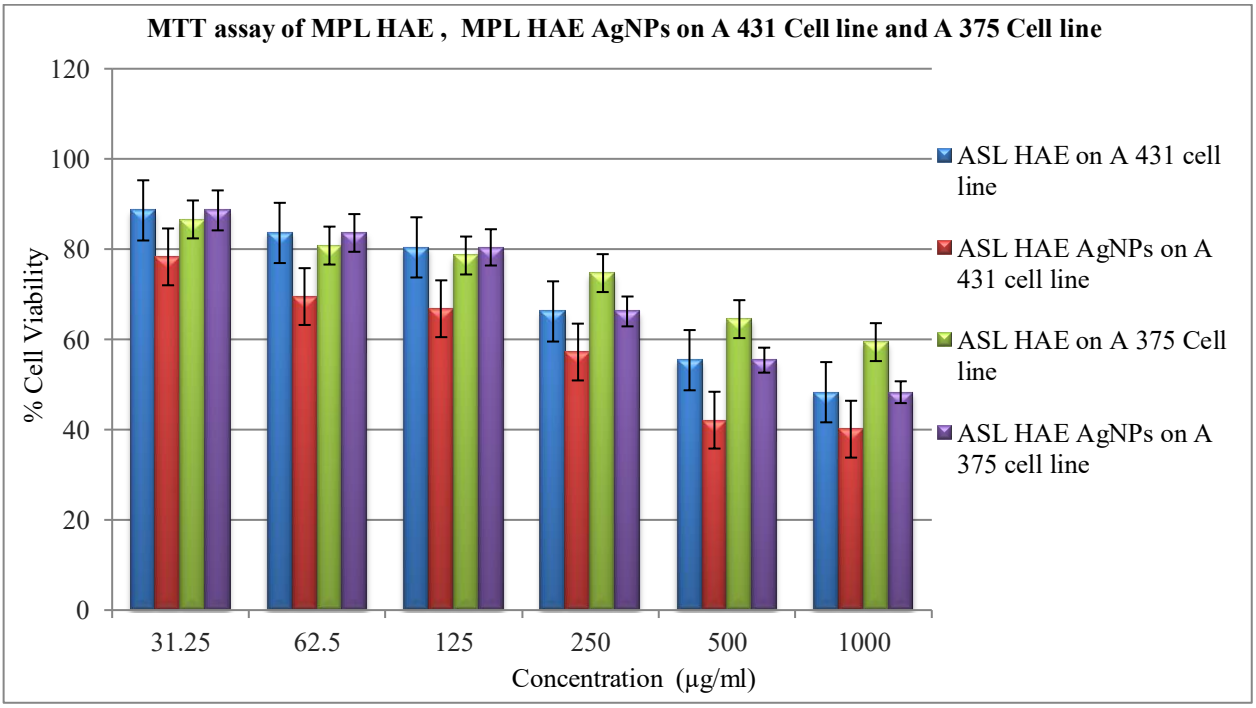

Figure 12: MTT assay of ASL HAE, AgNP's on A 431 and 375 cell line

AgNPs and their anticancer effects No. 431 Cell viability was recorded as 89.8%, 87.6%, 85.4%, 75.6%, 47.7%, and 44.81% at concentrations of 31.25, 62.5, 125, 250, 500, and 1000 µg/ml, respectively, as shown in Table 7. *Annona squamosa* Hydroalcpholic extract NPs had a half maximum inhibitory concentration of 570.2 µg/ml. In addition, AgNPs outperform the standard extract in terms of activity.

Anticancer Effect of Annona squamosa Hydroalcoholic Extract on Skin Cancer Cell Lines A375

According to Table 7, the cell viability was 86.6%, 80.8%, 78.6%, 74.7%, 64.5%, and 59.4% at doses of 31, 25, 6, 12, 5, 250, 500, and 1000 µg/ml of *Annona squamosa* Hydroalcoholic extract, which had an anticancer impact on skin cancer cell lines A375. Therefore, at a concentration of 1634 µg/ml, the hydroalcoholic extract of *Annona squamosa* exhibited half of its peak inhibitory concentration.

Anticancer Effect of Annona squamosa Hydroalcoholic Extract NPs on Skin Cancer Cell Lines A375

The cell viability was 80.4%, 83.6%, 88.6%, 66.2%, 55.4%, and 48.3% sequentially when skin cancer cell lines A375 were treated with *Annona squamosa* hydroalcoholic extract NPs at doses of 31, 25, 6, 12, 25, 250, 500, and 1000 µg/ml, as shown in Table 7. The value of 841.3 µg/ml was therefore determined to be the half maximum inhibitory concentration of the hydroalcholic extract NPs of *Annona squamosa*.

Figure 11 represents (a) for Normal control cell line observed under microscope for Cell viability. When it treat with *Annona squamosa* HAE (b) there is reduction in cell viability as well decrease size of Cancerous cell line A 431. When it treats with *Annona squamosa* HAE AgNPs (c) there is reduction in cell viability as compared to HAE (Hydroalcoholic extract) as well decrease size of Cancerous cell line A 431. Fig 11 (d) represent Effect *Annona squamosa* HAE on A 375 cell line, there is reduction in cell viability as well decrease size of Cancerous cell. Fig 11 (e) represent Effect *Annona squamosa* HAE AgNPs on A 375 cell line, there is reduction in cell viability as well decrease size of Cancerous cell as compared to hydroalcoholic extract.

The overall results for *In vitro* Skin Cancer Cell Line Activity are depicted in Figure 12.

CONCLUSION

Design Expert software streamlines optimization compared to conventional methods by using Central Composite Design to optimize key variables like 1mM $AgNO_3$, 0.1% *Annona squamosa* extract, 90 minutes reaction time, and 700 rpm stirring speed. Maximum yield occurred at medium extract and silver nitrate concentrations, with yields unaffected by stirring speed or time. AgNPs sized 105–508 nm were synthesized, with phenolic, Flavanoids and Tannin compounds playing a key role in their formation and stability. The antibacterial properties of AgNPs are due to the fact that they discharge silver ions continuously, which break down bacterial cell walls, render enzymes inactive, cause DNA damage via reactive oxygen species, and halt the creation of proteins. Nanoparticles less than 10 nm in size have a greater ability to penetrate the cell walls of Gram-negative bacteria, making them more vulnerable. *Annona squamosa* extracts showed enhanced antimicrobial effects when converted to AgNPs due to synergistic interactions between silver ions and phytochemicals. Regarding anticancer activity, *Annona squamosa* extract showed dose-dependent cytotoxicity on skin cancer cell lines A431 and A375, with stronger effects on A431 cells. Nanoparticles generally exhibited higher IC_{50} values, indicating differing cytotoxic effects depending on composition of nanoformulation and cell type.

REFERENCES

1. Sosna-Głębska A, Szczecińska N, Znajdek K, Sibiński M. Review on metallic oxide nanoparticles and their application in optoelectronic devices. Acta Innovations. 2019(30):5-15. https://doi.org/10.32933/ActaInnovations.30.1
2. Reddy KT Kumar, Dharmamoorthy G, Vasavi Devi D, Vidiyala N, Bagade OM, Elumalai S, Sagar Dantinapalli VL, Kasimedu S. Phytoconstituent Based Green Synthesis of Nanoparticles: Sources and Biomedical Applications in Cancer Therapy. Asian Journal of Green Chemistry. 2025;9(3):329-354. Doi: 10.48309/AJGC.2025.501113.1669
3. Moussa AY, Siddiqui SA, Elhawary EA, Guo K, Anwar S, Xu B. Phytochemical constituents, bioactivities, and applications of custard apple (*Annona squamosa* L.): A narrative review. Food Chemistry. 2024:140363. doi: 10.1016/j.foodchem.2024.140363.
4. Narwade DA, Aher AN. A review on: phytochemical and pharmacological study of *Annona squamosa*. PharmaTutor. 2019;7(1):5-10.
5. Sharma P, Mehta M, Dhanjal DS, Kaur S, Gupta G, Singh H, Thangavelu L, Rajeshkumar S, Tambuwala M, Bakshi HA, Chellappan DK. Emerging trends in the novel drug delivery approaches for the treatment of lung cancer. Chemico-biological interactions. 2019 Aug 25;309:108720. doi: 10.1016/j.cbi.2019.06.033
6. Utreja P, Jain S, K Tiwary A. Novel drug delivery systems for sustained and targeted delivery of anti-cancer drugs: current status and future prospects. Current Drug Delivery. 2010;7(2):152-61. doi: 10.2174/156720110791011783.
7. Gomes HI, Martins CS, Prior JA. Silver nanoparticles as carriers of anticancer drugs for efficient target treatment of cancer cells. Nanomaterials. 2021;11(4):964.
8. Hussein HA, Abdullah MA. Novel drug delivery systems based on silver nanoparticles, hyaluronic acid, lipid nanoparticles and liposomes for cancer treatment. Applied Nanoscience. 2022;12(11):3071-96. https://doi.org/10.1039/C4RA12784F
9. Vivek R, Thangam R, Muthuchelian K, Gunasekaran P, Kaveri K, Kannan S. Green biosynthesis of silver nanoparticles from *Annona squamosa* leaf extract and its *In vitro* cytotoxic effect on MCF-7 cells. Process Biochemistry. 2012;47(12):2405-10.
10. Hussein, A.A., Abd El-latif, M.B., Saad El-Din, M.I., El-Shenawy, N.S., Hammam, O. and Ibrahim, A.M., 2024. The molluscicidal activity of green synthesized

copper oxide–based *Annona squamosa* seed extract nanoparticles on the feeding behavior, biochemical, molecular, and immunohistochemical alterations of Biomphalariaalexandrina snails. Biological Trace Element Research, 202(5), pp.2327-2337.
11. Raja S, Ramesh V, Thivaharan V. Green biosynthesis of silver nanoparticles using Calliandrahaematocephala leaf extract, their antibacterial activity and hydrogen peroxide sensing capability. Arabian journal of chemistry. 2017;10(2):253-61.
12. Lokeshvar R, Ramaiyan V, Nithin V, Pavani S, Vinod Kumar T. Nanotechnology-driven therapeutics for liver cancer: Clinical applications and pharmaceutical insights. Asian Journal of Pharmaceutical and Clinical Reseacrh. 2025;18(2):8-26. https://doi.org/10.22159/ajpcr.2025v18i2.53429.
13. Ali IAM, Ahmed AB, Al-Ahmed HI. Green synthesis and characterization of silver nanoparticles for reducing the damage to sperm parameters in diabetic compared to metformin. Scientific Reports. 2023;13(1):2256. doi: 10.1038/s41598-023-29412-3.
14. Gamboa SM, Rojas ER, Martinez VV, Vega-Baudrit JJ. Synthesis and characterization of silver nanoparticles and their application as an antibacterial agent. International Journal of Biosensors & Bioelectronics. 2019;5(5):166-73. DOI:10.15406/ijbsbe.2019.05.00172
15. Meikle T, Dyett BP, Strachan JB, White J, Drummond CJ, Conn CE. Preparation, characterization, and antimicrobial activity of cubosome encapsulated metal nanocrystals. ACS Applied Material Interfaces. 2020;12(6):6944–6954. doi:10.1021/acsami.9b21783
16. Yadav J, Tare H. Silver Nanoparticles as Antimicrobial Agents: Mechanisms, Challenges, and Applications. International Journal of Pharmaceutical Quality Assurance. 2024;15(1):546-553. https://doi.org/10.25258/ijpqa.15.1.82
17. Urnukhsaikhan E, Bold BE, Gunbileg A, Sukhbaatar N, Mishig-Ochir T. Antibacterial activity and characteristics of silver nanoparticles biosynthesized from Carduus crispus. Scientific reports. 2021;11(1):21047. https://doi.org/10.1038/s41598-021-00520-2
18. Marzi M, Osanloo M, Vakil MK, Mansoori Y, Ghasemian A, Dehghan A, Zarenezhad E. Applications of metallic nanoparticles in the skin cancer treatment. BioMed Research International. 2022;2022(1):2346941. https://doi.org/10.1155/2022/2346941
19. Zeng L, Gowda BJ, Ahmed MG, Abourehab MA, Chen ZS, Zhang C, Li J, Kesharwani P. Advancements in nanoparticle-based treatment approaches for skin cancer therapy. Molecular Cancer. 2023;22(1):10. https://doi.org/10.1186/s12943-022-01708-4.
20. Bahraminasab M, Arab S, Jahan A. Adaptation of MC3T3 cell line to Dulbecco's Modified Eagle's medium. Tissue and Cell. 2020;64:101341.
21. Zhou P, An T, Zhao C, Li Y, Li R, Yang R, Wang Y, Gao X. Lactosylated PLGA nanoparticles containing ϵ-polylysine for the sustained release and liver-targeted delivery of the negatively charged proteins. International journal of pharmaceutics. 2015 ;478(2):633-43.
22. Hamdi OH, Saadedin SM, Al_Zaidi IH. Green biosynthesis of silver nanoparticles using gallium aparine green part extract and anti-skin cancer activity. Medico legal Update. 2021;21(2):908-13.
23. Li CC, Yu FS, Fan MJ, Chen YY, Lien JC, Chou YC, Lu HF, Tang NY, Peng SF, Huang WW, Chung JG. Anticancer effects of cantharidin in A431 human skin cancer (Epidermoid carcinoma) cells *In vitro* and in vivo. Environmental toxicology. 2017 ;32(3):723-38. doi: 10.1002/tox.22273.
24. Anith Jose R, Devina Merin D, Arulananth TS, Shaik N. Characterization analysis of silver nanoparticles synthesized from Chaetoceros calcitrans. Journal of Nanomaterials. 2022;2022(1):4056551. https://doi.org/10.1155/2022/4056551
25. Hassan H, Adam SK, Alias E, Meor Mohd Affandi MM, Shamsuddin AF, Basir R. Central composite design for formulation and optimization of solid lipid nanoparticles to enhance oral bioavailability of acyclovir. Molecules. 2021;26(18):5432. https://doi.org/10.3390/molecules26185432.